PAPER

# A hybrid method for the time-harmonic inverse acoustic transmission problem

To cite this article: João Paixão and Pedro Serranho 2025 *Phys. Scr.* **100** 045228

Physica Scripta

PAPER

# A hybrid method for the time-harmonic inverse acoustic transmission problem

RECEIVED
8 November 2024

REVISED
31 January 2025

ACCEPTED FOR PUBLICATION
3 March 2025

PUBLISHED
18 March 2025

**João Paixão**[1,2,*] **and Pedro Serranho**[1,2,3]

[1] Department of Sciences and Technology, Universidade Aberta, Rua da Escola Politécnica, 141-147, 1269-001 Lisbon, Portugal
[2] Center for Computational and Stochastic Mathematics (CEMAT), University of Lisbon, Av. Rovisco Pais 1, 1049-001 Lisbon, Portugal
[3] Coimbra Institute for Biomedical Imaging and Translational Research (CIBIT), Institute of Nuclear Sciences Applied to Health (ICNAS), University of Coimbra, 3000-548 Coimbra, Portugal
[*] Author to whom any correspondence should be addressed.

**E-mail:** jcpaixao@gmail.com **and** pedro.serranho@uab.pt

**Keywords:** inverse problem, acoustic transmission problem, hybrid method, iterative decomposition method, far-field data

## Abstract

The inverse transmission problem of scattering an acoustic wave by a penetrable object has several applications in various fields such as radar, sonar, geophysical exploration, medical imaging and non destructive testing. Here we propose a numerical hybrid method to inverse acoustic scattering by penetrable obstacles from far-field data in two-dimensions, that extends an iterative decomposition method to the transmission problem. The proposed method starts by reconstructing the scattered and interior field by imposing the far-field equation and one of the transmission conditions and, in the second step it uses the second transmission condition to update the position of the approximated boundary, by linearization. Also, we compared two approaches for the linearization step: a Newton-type method; and a gradient-type method with a penalty term for high oscillations of the solution. We also support the methods by a convergence result for a related optimization problem. Numerical results from eight incident directions show the method is feasible, though sensitive to noise.

## 1. Introduction

The time-harmonic far-field data inverse acoustic problem is to find the location and shape of the unknown obstacle that scatters one or more incident acoustic fields from the measurement of the asymptotic behavior of the scattered field, some examples of application can be found in [6, 8, 9, 15, 39]. Three major families of methods to solve inverse acoustic problems by impenetrable objects were developed over the last years [9], mainly since the 1960's with the work of Tikhonov about regularization schemes [40]. Decomposition methods [21–23] and Newton type methods [17, 20, 26] first and later Sampling and Probe methods [11, 33] gave interesting results and accurate reconstructions of the scatterer for several domain shapes. Decomposition methods break the inverse problem into two steps to deal separately with the ill-posed and non linear nature of the problem. Taking into account Rellich's lemma (e.g. [12]) that assures that the far-field data uniquely determines the scattered field, the method reconstructs the scattered field from the far-field pattern data in an ill-posed first step; then it finds the solution as the location where the boundary condition is satisfied in a nonlinear second step. Instead, Newton type methods rely on the linearization of the operator that maps the boundary condition to the far-field, dealing in an iterative way with the ill-posedness and nonlinearity of the map at the same time. Reconstructions are usually better than decomposition methods. However, in each iteration it is necessary to solve a set of direct problems to get the boundary update, which has a higher computational cost. Hybrid methods [18, 30, 31, 36, 37] appeared as a combination of these two methods, being able to deal with ill-posedness and nonlinearity in two different steps in each iteration to get good reconstructions with a low computational cost. The hybrid method can be seen as an iterative decomposition method, in the sense that it reconstructs the scattered field from the far-field data in a first step and then linearizes the reconstructed field to update the boundary from the boundary equation, iterating both steps until some stopping criteria is achieved.

Concerning inverse acoustic problems by penetrable objects, that is inverse transmission problems, Newton type methods [2, 32], or sampling methods [14, 19] were used with effectiveness, but decomposition methods cannot be applied to this case since they would need to reconstruct both the scattered and interior field from the far-field data without knowing the exact position of the boundary of the obstacle. Our aim in this paper is to extend the hybrid method for the transmission problem, with the necessary adaptations having in mind that this implies iterating a decomposition method at each step. As a general gist of the proposed method, at each iteration, the proposed hybrid method considers a current approximation of the boundary of the scatterer. Then, as a decomposition method, the scattered field is reconstructed from the far-field data and by imposing one of the transmission conditions at the current boundary, the interior field is reconstructed. In a second nonlinear step, one defines an operator that for fixed exterior and interior fields maps the current boundary approximation to the trace of the remaining transmission condition and solves the linearized equation in a Newton's method spirit. The two steps are iterated until some stopping criteria is achieved.

In a series of papers, Altundag and Kress [1–3] presented a procedure that also combines ideas of Newton's and decomposition methods using integral layer representations of the fields. However their approach is different from ours since it linearizes the layer representation as a boundary integral with respect to the boundary whilst in our method one linearizes the reconstructed fields. Lee [32] considers also a different approach that uses a Dirichlet-to-Newton map that transforms the problem into an exterior boundary value problem followed by an iterative method. Both make use of quadrature methods to discretize the layer potential's integral equations to numerically solve the problem.

Our paper is organized as follows. In section 2, we present the transmission problem and the ansatz for the solutions of the problem, also addressing how we obtain the synthetic far-field data for the input of the inverse transmission problem. In section 3, we present a related optimization problem and prove a convergence result to support our approach. In section 4, we introduce the hybrid method and detail its application. In section 5, we present some numerical results of the method. Finally we will discuss some conclusions and future directions of research.

## 2. The transmission problem

The Inverse Transmission Problem of scattering a time-harmonic acoustic wave by a penetrable obstacle in an homogeneous background medium consists in finding the location and shape of the scatterer $D$ from known far-field data. Paving the way to solve the inverse problem we will first spend some lines on the direct problem and a forward solver to set the foundation for our approach to numerically solve the given inverse scattering problem.

### 2.1. Direct problem

In time-harmonic low-frequency acoustic scattering the acoustic fields are modelled usually by the Helmholtz equation. The scattering of an incident plane field $u^i$ by a penetrable domain $D$ defined in an homogeneous background medium produces a scattered field $u^s$ outside the obstacle and an interior field $u_D$ inside the obstacle. The Transmission Problem models the impact of the presence of a penetrable obstacle $D$ with different sound velocity from the homogeneous background medium, and is defined as follows for the exterior field $u = u^i + u^s$ and interior field $u_D$.

**Problem 1.** Direct Problem Let $D \subset \mathbb{R}^2$, be a simply connected bounded open domain with a $C^2$ boundary. For a given incident plane field $u^i$, find the scattered field $u^s \in C^2(\mathbb{R}^2\setminus\bar{D}) \cap C(\mathbb{R}^2\setminus D)$ and the interior field $u_D \in C^2(D) \cap C(\bar{D})$ satisfying

$$\Delta u(x) + \kappa^2 u(x) = 0,\ x \in \mathbb{R}^2\setminus\bar{D}, \tag{1}$$

$$\Delta u_D(x) + \kappa_D^2 u_D(x) = 0,\ x \in D, \tag{2}$$

$$u^i(x) + u^s(x) = \lambda u_D(x),\ x \in \partial D, \tag{3}$$

$$\frac{\partial u^i}{\partial \nu}(x) + \frac{\partial u^s}{\partial \nu}(x) = \frac{\partial u_D}{\partial \nu}(x),\ x \in \partial D, \tag{4}$$

where $\kappa$ and $\kappa_D$ are the correspondent wavenumbers for the exterior and the interior mediums, respectively, with $\kappa > 0$ and $\kappa_D \in \mathbb{C}$, $\mathrm{Re}(\kappa_D) > 0$ and $\mathrm{Im}(\kappa_D) > 0$, $\lambda = \frac{\kappa}{\kappa_D}$ is the transmission coefficient, $\nu$ is the unit outward normal vector and the normal derivative is defined as in [12], the Sommerfeld radiation condition for the scattered field is also required

$$\lim_{r\to\infty}\sqrt{r}\left(\frac{\partial u^s}{\partial r}-i\kappa u^s\right)=0,\quad r=|x|. \tag{5}$$

equations (1) and (2) represent the Helmholtz equation outside and inside the domain, respectively, and (3) and (4) are the transmission conditions.

Sommerfeld radiation condition (5) ensures uniqueness of the solution and forces the asymptotic behavior of the scattered field as an outgoing spherical wave as

$$u^s(x)=\frac{e^{i\kappa|x|}}{\sqrt{|x|}}\left\{u_\infty(\hat{x})+O\left(\frac{1}{|x|}\right)\right\},\ |x|\to\infty, \tag{6}$$

uniformly in all directions $\hat{x}\in\Omega$, with $\hat{x}=\frac{x}{|x|}$, where $u_\infty$ is the far-field pattern [12] defined in the unitary circumference centered at the origin, $\Omega$, and will be the given data for the inverse transmission problem ahead. For a uniqueness result for the direct problem we refer to [3], where a single layer potential was used to represent the solution and the problem is formulated as a boundary integral equation problem, provided that $\kappa$ is not a Dirichlet eigenvalue of the negative Laplacian for the domain D. In [10] we can find uniqueness and existence results for three dimensions.

We will use a combination of layer potentials as a representation for the unknown fields

$$u^s(x)=\int_{\partial D}\frac{\partial\Phi(x,y)}{\partial\nu(y)}\varphi_1(y)+\Phi(x,y)\varphi_2(y)\quad \mathrm{d}s(y),\quad x\in\mathbb{R}^2\backslash\overline{D}, \tag{7}$$

$$u_D(x)=\int_{\partial D}\frac{\partial\Phi_D(x,y)}{\partial\nu(y)}\varphi_1(y)+\lambda\Phi_D(x,y)\varphi_2(y)\quad \mathrm{d}s(y),\quad x\in D, \tag{8}$$

where the fundamental solution $\Phi_\kappa$ to the Helmholtz equation in $\mathbb{R}^2$ is defined by

$$\Phi_\kappa(x,y):=\frac{i}{4}H_0^{(1)}(\kappa|x-y|), \tag{9}$$

and $H_0^{(1)}$ is the Hänkel function of first kind and order zero [12]. The fundamental solution $\Phi_\kappa(\cdot,y)$ is a radiant solution to the Helmholtz equation (with wavenumber $\kappa$) in $\mathbb{R}^2\backslash\{y\}$.

Assuming one incident plane field $u^i(x)=e^{i\kappa x\cdot d}$, $x\in\mathbb{R}^2\backslash D$ with direction $d$, the combined layer potentials are solutions to the transmission problem 1, provided $\varphi_j, j=1,2$ are solutions to the boundary integral equations

$$(1+\lambda)\varphi_1+2(K-\lambda K_D)\varphi_1+2(S-\lambda^2S_D)\varphi_2=-2e^{i\kappa x\cdot d} \tag{10}$$

$$(1+\lambda)\varphi_2-2(T-T_D)\varphi_1-2(K^*-\lambda K_D^*)\varphi_2=2i\kappa d\cdot\nu(x)e^{i\kappa x\cdot d}, \tag{11}$$

in terms of the standard layer potentials $S, K, K^*: C(\partial D)\to C(\partial D)$ and $T: C^{1,\alpha}(\partial D)\to C(\partial D)$, as defined in [12] by

$$\begin{aligned}(S\varphi)(x)&:=\int_{\partial D}\Phi(x,y)\varphi(y)\mathrm{d}s(y),\ x\in\partial D,\\ (K\varphi)(x)&:=\int_{\partial D}\tfrac{\partial\Phi(x,y)}{\partial\nu(y)}\varphi(y)\mathrm{d}s(y),\ x\in\partial D,\\ (K^*\varphi)(x)&:=\int_{\partial D}\tfrac{\partial\Phi(x,y)}{\partial\nu(x)}\varphi(y)\mathrm{d}s(y),\ x\in\partial D,\\ (T\varphi)(x)&:=\tfrac{\partial}{\partial\nu(x)}\int_{\partial D}\tfrac{\partial\Phi(x,y)}{\partial\nu(y)}\varphi(y)\mathrm{d}s(y),\ x\in\partial D.\end{aligned}$$

The corresponding far-field for the scattered field can then be defined by

$$u_\infty(\hat{x})=\frac{e^{\frac{i\pi}{4}}}{\sqrt{8\kappa\pi}}((K_\infty\varphi_1)(\hat{x})+(S_\infty\varphi_2)(\hat{x})),\ \hat{x}=\frac{x}{|x|}. \tag{12}$$

with the far-field layer potentials defined by

$$\begin{aligned}(S_\infty\varphi)(\hat{x})&=\int_{\partial D}e^{-i\kappa\hat{x}\cdot y}\varphi(y)\mathrm{d}s(y),\\ (K_\infty\varphi)(\hat{x})&=-i\kappa\int_{\partial D}(\hat{x}\cdot\nu(y))e^{-i\kappa\hat{x}\cdot y}\varphi(y)\mathrm{d}s(y).\end{aligned}$$

For the numerical solution one can consider the quadrature rules in [27, 28] as applied in [12, 25, 30].

### 2.2. Inverse transmission problem

The inverse problem can be stated as follows and this will be our problem of interest throughout the rest of the paper.

**Problem 2.** Under the same conditions of Problem 1, given the far-field patterns $u_{\infty,1}$, $u_{\infty,2},\ldots,u_{\infty,n_d}$ of the scattered fields $u_1^s$, $u_2^s,\ldots,u_{n_d}^s$ for a finite number $n_d$ of directions $d_1$, $d_2,\ldots,d_{n_d}$ of plane incident fields and the interior and exterior wavenumbers $\kappa_D$ and $\kappa$, respectively, determine the position and shape of the scatterer $D$.

For positive wavenumbers, Isakov [16] proved uniqueness for the inverse transmission problem in $\mathbb{R}^2$ and in $\mathbb{R}^3$. Later Kirsch and Kress [24] simplified Isakov's proof and Ramm [35] proved the uniqueness of $D$, $\lambda$ and $\kappa_D$. For complex wavenumbers we refer to [3], where a proof for a dielectric disk is presented. Also, it can be shown that in the conditions of Problem 1 and 2, there are no transmission eigenvalues [3, 41]. The inverse transmission problem is ill-posed, since the solution does not depend continuously on the data, which means that little perturbations in far-field data might result in major changes in the solution. In this way, having in mind that in applications measurement data is affected by errors, the numerical methods considered for problem at hand must consider stable ways to numerically solve the problem. Also, as the inverse problem is nonlinear, this has to be also taken into account for the numerical solution. In the next section we will introduce an optimization problem that is related with the proposed hybrid method for impenetrable obstacles.

## 3. A related optimization problem

The inverse transmission problem 2 can be expressed in terms of an optimization problem that provides a general convergence support for the proposed methods in the next section.

We consider the boundary of the solution to be in the space of star shaped curves

$$\gamma_r = \{z(t) = r(t)(\cos t,\ \sin t)\colon r \quad \text{is} \quad 2\pi\text{-periodic}\}, \tag{13}$$

where $r \in U$, with

$$U = \{r \in H^l([0,\ 2\pi])\colon 0 < r_1 \leqslant r(t) \leqslant r_2 \wedge r_1' \leqslant r'(t) \leqslant r_2',\ t \in [0,\ 2\pi]\}$$

where $r_1,\ r_2 \in \mathbb{R}^+$, $r_1',\ r_2' \in \mathbb{R}$ and $\varphi_j \in H^q(\gamma_r)$, for $j = 1, 2$ and $r' \in V$,

$$V = \{r'\colon r \in U\},$$

considering $q > \frac{3}{2} + \alpha$ $(0 < \alpha \leqslant 1)$ and $l > \frac{5}{2}$ for the following theoretical results.From equations (3), (4), (12) and the layer potential representation, one can formulate the inverse transmission problem as a minimization problem of the regularized cost function

$$\begin{aligned}\Lambda(\varphi_1,\ \varphi_2,\ r;\ \eta_1,\ \eta_2) = \|F_{\infty,\gamma_r}\varphi - u_\infty\|^2_{L^2(\Omega)} + \|B_{D,\gamma_r}\varphi + f_1\|^2_{L^2(\gamma_r)} + \|B_{N,\gamma_r}\varphi - f_2\|^2_{L^2(\gamma_r)} + \\ + \eta_1\|\varphi_1\|^2_{H^q(\gamma_r)} + \eta_1\|\varphi_2\|^2_{H^q(\gamma_r)} + \eta_2\|r'\|^2_{H^{l-1}([0,2\pi])},\end{aligned} \tag{14}$$

for $\eta_1, \eta_2 > 0$, where

$$\begin{aligned}F_{\infty,\gamma_r}\varphi &= K_{\infty,\gamma_r}\varphi_1 + S_{\infty,\gamma_r}\varphi_2,\\ B_{D,\gamma_r}\varphi &= (1+\lambda)\varphi_1 + 2(K - \lambda K_D)\varphi_1 + 2(S - \lambda^2 S_D)\varphi_2,\\ B_{N,\gamma_r}\varphi &= (1+\lambda)\varphi_2 - 2(T - T_D)\varphi_1 - 2(K^* - \lambda K_D^*)\varphi_2,\end{aligned}$$

with $\varphi$ representing the pair $(\varphi_1, \varphi_2)$, $f_1(x) = 2e^{i\kappa x\cdot d}$, $f_2(x) = 2i\kappa d\cdot\nu(x)e^{i\kappa x\cdot d}$. The first term in the cost function (14) forces the far-field equation, the second and third terms force the boundary conditions, the fourth and fifth stabilize the ill-posedness of the forward solver and the last term penalizes high oscillations of the solution.

We define the parametrization $r_0$ to be optimal if there exists a triplet $(\varphi_{1,0}, \varphi_{2,0}, r_0)$ that minimizes $\Lambda(\varphi_1, \varphi_2, r; \eta_1, \eta_2)$ over $H^q(\gamma_r) \times H^q(\gamma_r) \times U$, i.e.

$$\Lambda(\varphi_{1,0},\ \varphi_{2,0},\ r_0;\ \eta_1,\ \eta_2) = m(\eta_1,\ \eta_2),$$

with

$$m(\eta_1,\ \eta_2) = \inf_{\varphi_1 \in H^q(\gamma),\varphi_2 \in H^q(\gamma), r\in U} \Lambda(\varphi_1,\ \varphi_2,\ r;\ \eta_1,\ \eta_2).$$

We start by showing existence of an optimal solution, for the following regularity assumptions.

**Theorem 3.** *Consider $q > \frac{3}{2} + \alpha$, $0 < \alpha \leqslant 1$ and $l > \frac{5}{2}$. Then for each pair $(\eta_1, \eta_2)$ there exists an optimal $r_0 \in U$.*

**Proof.** We follow the same steps of [36, thm.6]. Suppose that the vector $(\varphi_{1,n}, \varphi_{2,n}, r_n)$ is a minimizing sequence of $\Lambda(\varphi_1, \varphi_2, r; \eta_1, \eta_2)$, i.e.

$$\lim_{n\to\infty} \Lambda(\varphi_{1,n},\ \varphi_{2,n},\ r_n;\ \eta_1,\ \eta_2) = m(\eta_1,\ \eta_2).$$

Since $U$ is bounded and $r \in H^l([0, 2\pi])$ with $l > \frac{5}{2}$, by the Sobolev compact embedding $H^l([0, 2\pi]) \subset C^2([0, 2\pi])$, $U$ is compact in $C^2([0, 2\pi])$. Also, $V$ is bounded and $r' \in H^{l-1}([0, 2\pi])$ with $l - 1 > \frac{3}{2}$ whence, again by the Sobolev compact embedding $H^{l-1}([0, 2\pi]) \subset C^1([0, 2\pi])$, $V$ is compact in $C^1([0, 2\pi])$.

Therefore, without loss of generality, by the closeness of both sets, as $n \to \infty$ we can assume $C^2([0, 2\pi])$-convergence of $r_n \to r_0$ in $U$ and $C^1([0, 2\pi])$-convergence of $r_n' \to r_0'$ in $V$.

For $\eta_1 > 0$ and $\eta_2 > 0$ we have

$$\eta_1 \|\varphi_{1,n}\|^2_{H^q(\gamma_r)} + \eta_1 \|\varphi_{2,n}\|^2_{H^q(\gamma_r)} + \eta_2 \|r_n'\|^2_{H^{l-1}([0,2\pi])} \leqslant \Lambda(\varphi_{1,n}, \varphi_{2,n}, r_n; \eta_1, \eta_2).$$

As $n \to \infty$

$$\Lambda(\varphi_{1,n}, \varphi_{2,n}, r_n; \eta_1, \eta_2) \to m(\eta_1, \eta_2),$$

there exist an $N$ and an $M$, such that for $n > N$ we have

$$\eta_1 \|\varphi_{1,n}\|^2_{H^q(\gamma_r)} + \eta_1 \|\varphi_{2,n}\|^2_{H^q(\gamma_r)} + \eta_2 \|r_n'\|^2_{H^{l-1}([0,2\pi])} \leqslant M,$$

by the definition of limit and the fact that $m(\eta_1, \eta_2)$ exists, and so $\varphi_{j,n}, j = 1, 2$ are bounded sequences in $H^q(\gamma_r)$ $\left(q > \frac{3}{2} + \alpha\right)$ and by the Sobolev embedding $H^q(\gamma_r) \subset C^{1,\alpha}(\gamma_r)$ one can assume subsequences $\varphi_{j,n} \to \varphi_{j,0}$.

Then by continuity of the functional $\Lambda$ in all its variables, the result follows

$$m(\eta_1, \eta_2) = \lim_{n\to\infty} \Lambda(\varphi_{1,n}, \varphi_{2,n}, r_n; \eta_1, \eta_2) = \Lambda(\varphi_{1,0}, \varphi_{2,0}, r_0; \eta_1, \eta_2).$$

□

We now head to prove the convergence of the solution to the inverse problem as $\eta_{j,n} \to 0, j = 1, 2$. To this end, we need to extend theorem 5.16 in [12] to our particular case, as follows.

**Theorem 4.** *Let $\Gamma_n$ represent a sequence of star like $C^2$ surfaces which converges with respect to the $C^{1,\alpha}$ norm to a $C^2$ surface $\Gamma$ as $n \to \infty$ and let $u_n$ and $u$ be radiating solutions to the Helmholtz equation in the exterior of $\Gamma_n$ and $\Gamma$ and $u_{D,n}$ and $u_D$ be solutions to the Helmholtz equation in the interior, of $\Gamma_n$ and $\Gamma$, respectively. Assume that the continuous boundary values of $u_n$ and $u_{D,n}$ on $\Gamma_n$, are $L^2$ convergent to the boundary values of $u$ and $u_D$ on $\Gamma$, respectively. The sequence $u_n$, together with all its derivatives, converges to $u$ uniformly on compact subsets of the open exterior of $\Gamma$, same with the sequence $u_{D,n}$ in the interior of $\Gamma$.*

**Proof.** Assuming the solutions (7) and (8) to the direct transmission problem, after parametrization on $\gamma_r$, setting $\psi_{j,r}(t) = \varphi_j(z(t)), g_{1,r}(t) = g_1(z(t))$ and $g_{2,r}(t) = g_2(z(t))$, the system of equations (10)–(11) can be written as

$$\chi - A_r \chi = g_r,$$

where

$$A_r = \frac{2}{1+\lambda}\begin{pmatrix} K_r - \lambda K_{D,r} & S_r - \lambda^2 S_{D,r} \\ -T_r + T_{D,r} & -K^*_r + \lambda K^*_{D,r} \end{pmatrix},$$

$$\chi = \begin{pmatrix} \psi_{1,r} \\ \psi_{2,r} \end{pmatrix},$$

and

$$g_r = \begin{pmatrix} g_{1,r} \\ g_{2,r} \end{pmatrix}.$$

By the Fréchet differentiability [12, 34] of $A_r$ components

$$\|A_{r_n} - A_r\|_\infty \leqslant C_r \|r_n - r\|_{1,\alpha},$$

defining

$$\|A_{r_n} - A_r\|_\infty := \max_{i,j=1,2} \{\|A_r^{ij}\|_\infty\}$$

for a constant $C_r$ depending on $r$, where $A^{i,j}$, $i, j = 1, 2$ denotes each of the four blocks of the matrix $A_r$. By the adjoint operators of each of the blocks in $A_r$, this inequality can be express also for the adjoint of $A_r$ in $L^2$

$$A_r^* = \frac{2}{1+\overline{\lambda}}\begin{pmatrix} -\overline{K}_r + \overline{\lambda}\overline{K}_{D,r} & (-\overline{T}_r + \overline{T}_{D,r}) S_0^2 \\ \overline{S}_r - \overline{\lambda^2}\overline{S}_{D,r} & \overline{K^*}_r - \overline{\lambda}\,\overline{K^*}_{D,r} \end{pmatrix},$$

since $\chi \in H^q([0, 2\pi]) \times H^q([0, 2\pi])$ we have that $\chi \in L^2([0, 2\pi]) \times L^2([0, 2\pi])$ by the Sobolev embedding. Then we have two adjoint bounded linear operators and $|(\psi_{1,r}, \psi_{2,r})| \leqslant \|\psi_{1,r}\| \|\psi_{2,r}\|$ in $L^2$, then by Lax's theorem one

can conclude that $A_r$ is bounded by the norm induced by the scalar product, so

$$\|A_{r_n} - A_r\|_{L^2([0,2\pi])} \leqslant C\|r_n - r\|_{1,\alpha}.$$

Also, from [24, 29] and since every Hölder continuous function in a bounded domain is in $L^2$ one concludes that $(I + A_{r_n})^{-1}$ exists and $\|(I + A_{r_n})^{-1}\|_{L^2([0,2\pi])}$ is bounded.

Since

$$(I + A_{r_n})(\chi_{r_n} - \chi_r) = f_{r_n} - f_r - (A_{r_n} - A_r)\chi_r$$

one has

$$\|\chi_{r_n} - \chi_r\|_{L^2([0,2\pi])} = \|(I + A_{r_n})^{-1}\|_{L^2([0,2\pi])}\|f_{r_n} - f_r - (A_{r_n} - A_r)\chi_r\|_{L^2([0,2\pi])}$$

$$\|\chi_{r_n} - \chi_r\|_{L^2([0,2\pi])} \leqslant C'(\|f_{r_n} - f_r\|_{L^2([0,2\pi])} + \|(A_{r_n} - A_r)\|_{L^2([0,2\pi])}\|\chi_r\|_{L^2([0,2\pi])})$$

with $\|\chi_r\|_{L^2([0,2\pi])} = \max\{\|\psi_{1,r}\|_{L^2([0,2\pi])}, \|\psi_{2,r}\|_{L^2([0,2\pi])}\}$.

Then we have convergence for the densities $\varphi_{j,n} \to \varphi_j$, $n \to \infty$ in $L^2$. Substituting in (7) and (8) one gets the convergence of $u_n$ and $u_{D,n}$, by applying the Cauchy–Schwartz inequality. □

**Theorem 5.** *Assume $q > \frac{3}{2} + \alpha$ and $l > \frac{5}{2}$. Let $\mathrm{n} \to \infty$, $\eta_{\mathrm{j,n}} \to 0$, $\mathrm{j} = 1, 2$ and $\mathrm{r_n}$ an optimal sequence. Suppose also that the solution $\Gamma$ to the inverse transmission problem can be parameterized by some $\mathrm{r}_\Gamma \in \mathrm{U}$. Then there exists a convergent subsequence of $\mathrm{r_n}$. If $\mathrm{u}_\infty$ is the exact far-field of the exterior solution $\mathrm{u}$ of the direct transmission problem, then every limit point $\mathrm{r}_\delta$ represents a curve that is a solution to*

$$\begin{cases} u^s + u^i - \lambda u_D = 0 \\ \frac{\partial u^s}{\partial \nu} + \frac{\partial u^i}{\partial \nu} - \frac{\partial u_D}{\partial \nu} = 0, \end{cases} \text{on} \quad \gamma_{r_\delta}. \tag{15}$$

**Proof.** The solution to the direct transmission problem (1), which is formulated as a combination of single and double layer potentials, is determined by the solutions to the boundary equations, denoted as $\varphi_j$, for $j = 1, 2$. It is assumed that $u_\infty$ represents the precise far-field. Then we have that

$$\|F_{\infty,\Gamma}\varphi - u_\infty\|^2_{L^2(\Omega)} = \|B_{D,\Gamma}\varphi + u^i\|^2_{L^2(\Gamma)} = \left\| B_{N,\Gamma}\varphi - \frac{\partial u^i}{\partial \nu} \right\|^2_{L^2(\Gamma)} = 0$$

And

$$m(\eta_1, \eta_2) \leqslant \Lambda(\varphi_1, \varphi_2, r_\Gamma; \eta_1, \eta_2) = \eta_1\|\varphi_1\|^2_{H^q(\Gamma)} + \eta_1\|\varphi_2\|^2_{H^q(\Gamma)} + \eta_2\|r_\Gamma'\|^2$$

implies that for $n \to \infty$

$$\lim_{\eta_{1,n}\to 0,\ \eta_{2,n}\to 0} m(\eta_{1,n}, \eta_{2,n}) = 0$$

By theorem 3, there exists a convergent subsequence of optimal $r_{k(n)}$. Denoting $k = k(n)$, let $r_\delta$ be the limit point of that convergent subsequence and let $u^\delta$ and $u^\delta_D$ be the solution to the direct transmission problem with boundary conditions (15) on $\gamma_\delta$.

As each $r_k$ is optimal, there exists $(\varphi_{1,k}, \varphi_{2,k}, r_k)$ that

$$\Lambda(\varphi_{1,k}, \varphi_{2,k}, r_k; \eta_{1,k}, \eta_{2,k}) = m(\eta_{1,k}, \eta_{2,k})$$

Taking $u^s_k$ and $u_{D,k}$ the solution for the direct transmission problem for $\gamma_k$ with densities $(\varphi_{1,k}, \varphi_{2,k})$, one has

$$\|u^s_k - \lambda u_{D,k} + u^i\|^2_{L^2(\gamma_k)} \leqslant m(\eta_{1,k}, \eta_{2,k}) \to 0, \tag{16}$$

$$\left\| \frac{\partial u^s_k}{\partial \nu} - \frac{\partial u_{D,k}}{\partial \nu} + \frac{\partial u^i}{\partial \nu} \right\|^2_{L^2(\gamma_k)} \leqslant m(\eta_{1,k}, \eta_{2,k}) \to 0, \tag{17}$$

$$\|F_{\infty,\Gamma}\varphi_k - u_\infty\|^2_{L^2(\Omega)} \leqslant m(\eta_{1,k}, \eta_{2,k}) \to 0. \tag{18}$$

By (16) $u_k - \lambda u_{D,k}$ converges to $u^\delta - \lambda u^\delta_D$ and, by theorem 4 the far-field pattern of $u_k$ also converges to the far-field pattern $u^\delta_\infty$ of $u^\delta$. From (18) one finally concludes that $u^\delta_\infty = u_\infty$. □

This convergence result for the given optimization problem supports our approach in a theoretical level, though there is a gap between this optimization and the actual application of the method. In fact, the proposed hybrid method splits the optimization in two steps, as detailed in the next section, while the convergence result is for the minimization of all unknowns simultaneously. We are now in a position to present the proposed generalization of the hybrid method for the inverse transmission problem.

## 4. The hybrid method

The hybrid method that we will generalize for the inverse transmission problem 2 can be seen as a combination of decomposition and Newton-type methods or as an iterative decomposition method. In fact, we will consider two approaches for the linearization, having this in mind.

At the iteration $n$ of the method, we consider the current approximation $\gamma_n$ for the boundary. In the spirit of a decomposition method, we start by recovering the scattered field $u^s$ and interior field $u_D$ from the far-field pattern $u_\infty$ and one of the two transmission conditions, namely the the Neumann condition (4). Though Rellich's lemma ensures that the reconstructed scattered field $u^s$ is uniquely determined by the far-field pattern $u_\infty$, the reconstructed interior field $u_D$, in general, will not be exact, since the transmission condition is imposed on an approximated boundary $\gamma_n$. Since the far-field equation is ill-posed, the use of Tikhonov regularization is advised. This first step corresponds to minimization the cost function

$$\begin{aligned}\tilde{\Lambda}_1(\varphi_{1,n},\,\varphi_{2,n};\,\eta_1,\,r_n) = \|F_{\infty,\gamma_r}\varphi_n - u_\infty\|^2_{L^2(\Omega)} + \|B_{N,\gamma_r}\varphi_n - f_2\|^2_{L^2(\gamma_n)} \\ + \eta_1\|\varphi_{1,n}\|^2_{L^2(\gamma_n)} + \eta_1\|\varphi_{n,2}\|^2_{L^2(\gamma_n)}\,,\end{aligned} \tag{19}$$

with the radial parametrization $r_n$ of $\gamma_n$ fixed. Then, in the spirit of a Newton-type method, in a second step one looks for the position where the remaining Dirichlet boundary condition (3) is satisfied, by linearization. This corresponds to minimizing the cost function

$$\tilde{\Lambda}_2(r;\,\eta_2,\,\varphi_{1,n},\,\varphi_{2,n}) = \|B_{D,\gamma_r}\varphi_n + f_1\|^2_{L^2(\gamma_r)} + \eta_2\|r'\|^2_{L^2([0,2\pi])}\,, \tag{20}$$

with the densities $(\varphi_{1,n},\varphi_{2,n})$ fixed. This defines an update of the boundary approximation $\gamma_{n+1}$ and one iterates both steps, repeating this process until a stopping criteria is fulfilled.

The second term in (20) stabilizes the solution $r$ but its presence prevents the application of Newton's method, since for $\eta_2 > 0$ the only solutions with vanishing cost function (20) are circumferences. Therefore, for the second step we will consider two numerical approaches. For $\eta_2 > 0$ we consider a gradient-type method, while for $\eta_2 = 0$ we will consider a Newton-type method in the spirit of the hybrid method for impenetrable obstacles [30, 31, 36, 37]. We also note there is a gap between the optimization problem in section 3 and this approach, since the minimization of $\Lambda$ in (14) is divided in two steps: the minimization of $\tilde{\Lambda}_1$ in (19) and the subsequent minimization of $\tilde{\Lambda}_2$ in (20).

### 4.1. Numerical implementation

To avoid an inverse crime [12], since the far-field synthetic data is generated by a combined single and double layer representation, we will consider representations by the method of fundamental solutions (MFS) in the inverse problem, namely considering the ansatz

$$\tilde{u}^s(x) \coloneqq \sum_{j=1}^{S} a_j \frac{i}{4} H_0^{(1)}(\kappa|x - s_j|), \quad x \in \mathbb{R}^2\backslash D, \tag{21}$$

$$\tilde{u}_D(x) \coloneqq \sum_{j=1}^{S_D} b_j \frac{i}{4} H_0^{(1)}(\kappa_D|x - s_{D,j}|), \quad x \in D, \tag{22}$$

where $s_j \in \mathcal{G}_1 \subset D, j = 1,\ldots,S$ and $s_{D,j} \in \mathcal{G}_2 \subset \mathbb{R}^2\backslash\overline{D}, j = 1,\ldots,S_D$ are the source points for the scattered field $u^s$ and the interior field $u_D$, respectively, and $\mathcal{G}_j$, $j = 1,\ 2$ are closed smooth curves. The set of linear combinations of fundamental solutions to the Helmholtz equation from different source points $y$ in a closed curve outside the domain is dense in the set of solutions of the Helmholtz equation [4, 38] so this motivates the use of linear combinations of fundamental solutions as ansatz for the approximation of the solution [5, 7, 13]. Moreover, computing the gradient of the fields needed for the second step at each iteration of our approach with an MFS representation is easier than considering the jump relations of the layer potentials, while assuming accuracy. Also, it is known that the correspondent far-field for the scattered field $\tilde{u}^s$ in (21) is given by

$$\tilde{u}_\infty(\hat{x}) = \frac{e^{i\frac{\pi}{4}}}{\sqrt{8\pi\kappa}} \sum_{j=1}^{S} a_j e^{-i\kappa s_j\cdot\hat{x}},\ \hat{x} \in \Omega. \tag{23}$$

Assuming one incident plane field $u^i(x) = e^{i\kappa x\cdot d}$, $x \in \mathbb{R}^2\backslash D$, with direction $d$, and a given current approximation $\gamma_n$ with radial parametrization $r_n$ for the exact boundary $\Gamma$ at iteration $n$, the first step of the hybrid method consists in solving the system of equations for $M$ far-field data points and $N$ collocation points over the boundary given by

$$\frac{e^{i\frac{\pi}{4}}}{\sqrt{8\pi\kappa}} \sum_{j=1}^{S} a_j e^{-i\kappa s_j\cdot\hat{x}_k} = \tilde{u}_\infty(\hat{x}_k),\ k = 1,\ldots,M, \tag{24}$$

$$\kappa\sum_{j=1}^{S} a_j \frac{(x_p - s_j)\cdot\nu(x)H_1^{(1)}(\kappa\mid x_p - s_j\mid)}{\mid x_p - s_j\mid} - \kappa_D\sum_{j=1}^{S_D} b_j \frac{(x_p - s_{D,j})\cdot\nu(x)H_1^{(1)}(\kappa_D\mid x_p - s_{D,j}\mid)}{\mid x_p - s_{D,j}\mid} = f(x_p),\ p = 1,\ldots,N, \tag{25}$$

by Tikhonov regularization to determine the coefficients $a_j, j = 1, \ldots, S$ and $b_j, j = 1, \ldots, S_D$, with $f(x) = 4\kappa d\cdot\nu(x)e^{i\kappa x\cdot d}$, where the artifical boundaries $\mathcal{G}_{1,n} \subset D$ and $\mathcal{G}_{2,n} \subset \mathbb{R}^2\backslash\overline{D}$ are chosen by scaling the radial parametrization inwards and outwards of the obstacle $D$, respectively. So that the system is overdetermined, one should consider $M + N \geqslant S + S_D$. This completes the first step of the hybrid method, that corresponds to minimizing (19).

For the second step one aims at minimizing (20), so, as previously mentioned, we will separate the approach in two cases: Newton-type method for $\eta_2 = 0$ and gradient-type method for $\eta_2 > 0$. We will consider that the radial parametrization $r$ in (13) is a trignometric polynomial given by

$$r(t) = \alpha_0 + \sum_{q=1}^{N_r} \alpha_q\cos(qt) + \beta_q\sin(qt), \tag{26}$$

with $2N_r + 1$ real coefficients to be determined.

*4.1.1. Second step: newton-type method ($\eta_2 = 0$):*
Let $G_D$: $\gamma \mapsto (\tilde{u} - \lambda\tilde{u}_D)|_\gamma$. It can be shown that $G_D$ is Fréchet differentiable [30, 36], with Fréchet derivative given by

$$G_D^{'}(\gamma)h = h\cdot\mathrm{grad}(\tilde{u} - \lambda\tilde{u}_D)|_\gamma$$

where the gradient of the field can be explicitly determined by differentiation of (21). As one wants to find the location where the Dirichlet boundary condition is satisfied, that is $\gamma$ such that $G(\gamma) = 0$. One linearizes this equation in a Newton's method spirit, at the current approximation $\gamma_n$, to solve

$$G_D^{'}(\gamma_n)h = -G_D(\gamma_n)$$

in order to obtain the new update parametrized $\gamma_{n+1} = \gamma_n + h$ with some abuse of notation, since the sum is made in the radial parametrization as $r_{n+1} = r_n + r_h$. We note that this is similar to finding the minimum of the cost function (20) in the case $\eta_2 = 0$, since in this case the minimum is found when $G_D(\gamma_n) = 0$. For more than one incident wave we solve simultaneously the correspondent linear systems.

**Remark 1.** Obstacle with unknown center We would like to remark that in the previous lines we considered that the parametrization of the boundary of the obstacle is given by

$$z(t) = r(t)(\cos(t),\ sin(t)),$$

which corresponds to a parametrization of the boundary centered at the origin. However, the Newton-type approach can be easily extended for the case where the center $c = (c_1,\ c_2) \in \mathbb{R}^2$ of the obstacle is unknown, namely by considering

$$z(t) = (c_1,\ c_2) + r(t)(\cos(t),\ sin(t)).$$

Note that in this case the derivatives in $c_1, c_2$ are simply given by each of the components of $\mathrm{grad}(\tilde{u} - \lambda\tilde{u}_D)|_\gamma$, so this can be easily incorporated in the minimization step.

*4.1.2. Second step: gradient-type method ($\eta_2 > 0$):*
In this case, the cost function (20) does not vanish in general. So instead of looking for vanishing roots of the cost function, one wants to find its minimum. Therefore, it makes sense to apply a gradient-type method directly to the cost function $\tilde{\Lambda}_2$ in (20). This can be obtained in terms of the partial derivatives of the cost function in terms of the parameters of the radial parametrization (26), that is,

$$\frac{\partial\tilde{\Lambda}_2}{\partial\alpha_q} = \frac{2\pi}{N}\sum_{p=1}^{N}\left\{2\mathcal{H}_1(z(t_p))\cdot\hat{x}(t_p)|z'(t_p)|\frac{\partial r(t_p)}{\partial\alpha_q} + \mathcal{H}_2(z(t_p))\frac{\partial\mid z'(t_p)\mid}{\partial\alpha_q} + \eta_2 r'(t_p)\frac{\partial r'(t_p)}{\partial\alpha_q}\right\},$$

$$\frac{\partial\tilde{\Lambda}_2}{\partial\beta_q} = \frac{2\pi}{N}\sum_{p=1}^{N}\left\{2\mathcal{H}_1(z(t_p))\cdot\hat{x}(t_p)|z'(t_p)|\frac{\partial r(t_p)}{\partial\beta_q} + \mathcal{H}_2(z(t_p))\frac{\partial\mid z'(t_p)\mid}{\partial\beta_q} + 2\eta_2 r'(t_p)\frac{\partial r'(t_p)}{\partial\beta_q}\right\},$$

where

$$\mathcal{H}_1(z(t_p)) = \mathrm{Re}((\tilde{u} - \lambda\tilde{u}_D)(z(t_p)))\mathrm{Re}(\mathrm{grad}(\tilde{u} - \lambda\tilde{u}_D)(z(t_p))) + \mathrm{Im}((\tilde{u} - \lambda\tilde{u}_D)(z(t_p)))\mathrm{Im}(\mathrm{grad}(\tilde{u} - \lambda\tilde{u}_D)(z(t_p)))$$

and

$$\mathcal{H}_2(z(t_p)) = \mathrm{Re}((\tilde{u} - \lambda\tilde{u}_D)(z(t_p)))^2 + \mathrm{Im}((\tilde{u} - \lambda\tilde{u}_D)(z(t_p)))^2$$

and

$$\frac{\partial r(t_p)}{\partial \alpha_0} = 1, \quad \frac{\partial r'(t_p)}{\partial \alpha_0} = 0, \quad \frac{\partial |z'(t_p)|}{\partial \alpha_0} = \frac{r(t_p)}{|z'(t_p)|}$$

and

$$\frac{\partial r(t_p)}{\partial \alpha_q} = q\cos(qt_p), \quad \frac{\partial r(t_p)}{\partial \beta_q} = q\sin(qt_p),$$
$$\frac{\partial r'(t_p)}{\partial \alpha_q} = -q\sin(qt_p), \quad \frac{\partial r'(t_p)}{\partial \beta_q} = q\cos(qt_p),$$
$$\frac{\partial\,|\,z'(t_p)\,|}{\partial \alpha_q} = \frac{r'(t_p)(-q\sin(qt_p)) + r(t_p)\cos(qt_p)}{|\,z'(t_p)\,|}$$
$$\frac{\partial\,|\,z'(t_p)\,|}{\partial \beta_q} = \frac{r'(t_p)(q\cos(qt_p)) + r(t_p)\sin(qt_p)}{|\,z'(t_p)\,|}$$

for $q = 1, \ldots N_r$, with

$$(\tilde{u} - \lambda\tilde{u}_D)(z(t_p)) = \sum_{j=1}^{S} a_j H_0^{(1)}(\kappa|z^n(t_p) - s_j|) - \sum_{l=1}^{S_D} \lambda b_l H_0^{(1)}(\kappa_D|z^n(t_p) - s_{D,l}|),$$

and

$$\mathrm{grad}(\tilde{u} - \lambda\tilde{u}_D)(z(t_p)) = -\frac{i}{4}\kappa\sum_{j=1}^{S} a_j \frac{H_1^{(1)}(\kappa\,|\,z(t_p) - s_j\,|)(z(t_p) - s_j)}{|\,z(t_p) - s_j\,|} + \frac{i}{4}\kappa_D\sum_{j=1}^{S_D} \lambda b_j \frac{H_1^{(1)}(\kappa_D\,|\,z(t_p) - s_{D,j}\,|)(z(t_p) - s_{D,j})}{|\,z(t_p) - s_{D,j}\,|}.$$

One then updates the position of the approximated boundary $\gamma_n$ to $\gamma_{n+1}$ in a least squares sense by considering a shift in the radial parametrization parameters (26) of $-\delta\ \mathrm{grad}(\tilde{\Lambda}_2)$ with some fixed factor $\delta > 0$. If one considers more than one incident wave, then the cost function is given by the sum of each of the cost functions for each incident direction.

In the next section we present some numerical results to illustrate the feasibility and performance of the method.

## 5. Numerical results

We now present some numerical results to illustrate the feasibility and accuracy of the hybrid method and to compare both approaches for the second step.

As in [1], we consider as data the far-field for 8 incident fields

$$u_j^i(x) = e^{i\kappa x\cdot d_j},\ j = 1,\ldots,8,$$

with different incidence directions $d_j = \left(\cos\left(\frac{2\pi j}{8}\right), \sin\left(\frac{2\pi j}{8}\right)\right), j = 1, \ldots, 8$. Our experiments showed that the method does not present consistent results with fewer incident directions. We considered a fixed wavenumber $\kappa = 1$ for the background, while we considered $\kappa_D = 2 + 3i$ for the scatterer medium in the first three examples. We also add example 5.1.1 to examine the influence of $\eta_2$ on the accuracy of reconstructions of the gradient type method and example 5.4 with an interior wavenumber $\kappa_D = 10 + 10i$ for the kite shaped obstacle.

As mentioned in section 4.1, to avoid an inverse crime, for each of the 8 incident directions the synthetic far-field data was computed in $M = 120$ equidistant points on the unit circumference $\Omega$ by the layer potentials representation (7)–(8) considering 64 collocation points at the exact boundary $\Gamma$, while for the inverse problem we considered 100 equidistant collocation points and an MFS representation (21)–(22) with $S = 100$, $S_D = 80$ source points over the artificial boundaries $\mathcal{G}_1$ and $\mathcal{G}_2$ obtained by scaling the radial parametrization $r_n$ by a factor of 0.9 and 1.1, respectively. To test the stability of the method we also added 1% and 2% noise in the maximum norm to the far-field data with a uniform distribution.

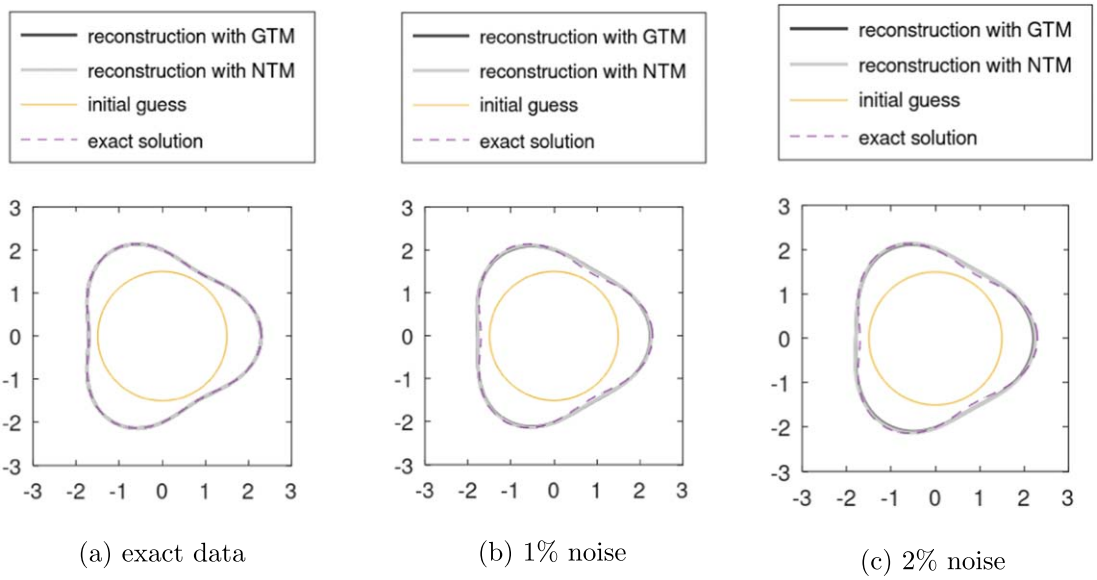


**Figure 1.** Reconstructions for the rounded corner triangle in section 5.1 by both approaches for the second step of the Hybrid method.

**Table 1.** Sequence of values of $\tilde{\Lambda}_2(\gamma_n)$ with respect to the iteration $n$ by the Newton-type method (NTM) and the gradient-type method (GTM) for the rounded corner triangle scatterer in section 5.1.

| | No noise | | 1% Noise | | 2% Noise | |
|---|---|---|---|---|---|---|
| $n$ | NTM | GTM | NTM | GTM | NTM | GTM |
| 1 | 88.88571 | 88.88571 | 53.52459 | 53.52459 | 53.56856 | 53.56856 |
| 2 | 9.60783 | 16.27506 | 2.01980 | 0.95438 | 2.25792 | 1.33625 |
| 3 | 0.01118 | 9.15335 | 0.80680 | 0.92095 | 1.24224 | 1.32915 |
| 4 | 0.00084 | 5.40017 | 0.81141 | 0.90362 | 1.31681 | 1.39479 |
| 5 | 0.00076 | 3.28564 | | 0.90362 | | |
| 6 | 0.00074 | 2.06037 | | 0.91397 | | |
| 10 | 0.00067 | 0.44938 | | | | |
| 15 | 0.00055 | 0.12212 | | | | |
| 20 | 0.00044 | 0.04133 | | | | |
| 25 | 0.00040 | 0.01452 | | | | |
| 30 | | 0.00562 | | | | |
| 34 | | 0.00480 | | | | |

In each iteration the first step is solved with a Tikhonov regularization with a regularization parameter $\eta_1 = 0.8^{n-1} \times 10^{-10}$ for exact data and $\eta_1 = 0.8^{n-1} \times 10^{-2}$ for noisy data. For the second step of the gradient-type method (GTM) the constrain for $r'$ in (20) is defined by $\eta_2 = 0.8^{n-1}$ for exact data and $\eta_2 = 0.8^{n-1} \times 10^{-1}$ for noisy data. Also we considered a parametrization space of the form (26) with $N_r \leqslant 20$. As the stopping criteria, we stop as soon as $\tilde{\Lambda}_2(\gamma_{n+1}) > \tilde{\Lambda}_2(\gamma_n)$, that is, as soon as the cost function (20) increases with $n$. We note that we considered the same parameters for all presented examples, not adapting them to each particular case, this strengths the robustness of the proposed method.

For each scatterer considered, each iterative approach considers the same initial guess for the different types of data: a circumference centered at the origin with radius 1.5. In all the following figures, the dashed red line represents the exact solution, the full blue line the initial guess, the thick green line the boundary reconstruction with the gradient-type method and the thick yellow line the boundary reconstruction with the Newton-type method.

### 5.1. Rounded corner triangle

We start by considering a domain inside the considered approximation space, that is the rounded corner triangle parametrized by

$$z(t) = (2 + 0.3\cos 3t)(\cos t, \sin t),\ t \in [2, \pi].$$

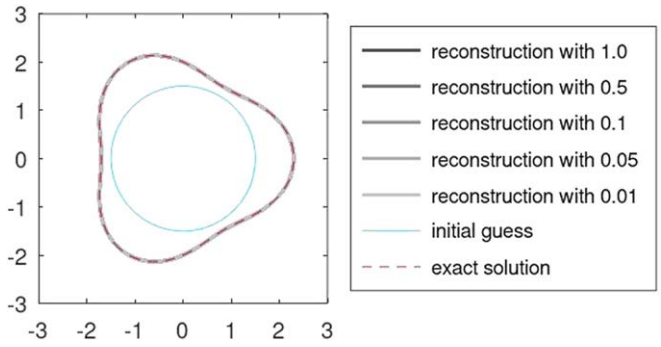


**Figure 2.** Reconstructions for the triangle scatterer in section 5.1 with different values for the constrain $\eta_2$ for the gradient-type method.

**Table 2.** Sequence of values of $\|B_D\varphi + u^i\|$ and $\tilde{\Lambda}_2$ with respect to iteration $n$ for different values of $\eta_2$ by the gradient-type method (GTM) for the triangle shape with no noise COLUMNSTYLESBEGIN=ES1lES2cES3cES4cES5c=COLUMNSTYLESEND.

| | $\eta_2 = 0.8^{n-1}$ | | $\eta_2 = 0.8^{n-1} \times 0.5$ | | $\eta_2 = 0.8^{n-1} \times 0.1$ | |
|---|---|---|---|---|---|---|
| $n$ | $\|B_D\varphi + u^i\|$ | $\tilde{\Lambda}_2$ | $\|B_D\varphi + u^i\|$ | $\tilde{\Lambda}_2$ | $\|B_D\varphi + u^i\|$ | $\tilde{\Lambda}_2$ |
| 1 | 88.88571 | 88.88571 | 88.88571 | 88.88571 | 88.88571 | 88.88571 |
| 2 | 15.43602 | 16.27506 | 15.43602 | 15.85554 | 15.43602 | 15.51992 |
| 3 | 8.26262 | 9.15335 | 8.11631 | 8.57933 | 8.00174 | 8.09722 |
| 4 | 4.57108 | 5.40017 | 4.41027 | 4.85178 | 4.28557 | 4.37840 |
| 5 | 2.55774 | 3.28564 | 2.41954 | 2.81315 | 2.31561 | 2.39942 |
| 10 | 0.16297 | 0.44938 | 0.12563 | 0.28240 | 0.11041 | 0.14418 |
| 15 | 0.02187 | 0.12212 | 0.00835 | 0.06198 | 0.00664 | 0.01799 |
| 20 | 0.00714 | 0.04133 | 0.00148 | 0.01935 | 0.00106 | 0.00477 |
| 25 | 0.00302 | 0.01452 | 0.00074 | 0.00666 | 0.00050 | 0.00171 |
| 29 | 0.00178 | 0.00655 | 0.00075 | 0.00319 | 0.00073 | 0.00123 |
| 30 | 0.00179 | 0.00562 | 0.00075 | 0.00270 | | |
| 32 | 0.00194 | 0.00441 | 0.00152 | 0.00277 | | |
| 33 | 0.00202 | 0.00399 | | | | |
| 34 | 0.00322 | 0.00480 | | | | |

| | $\eta_2 = 0.8^{n-1} \times 0.05$ | | $\eta_2 = 0.8^{n-1} \times 0.01$ | |
|---|---|---|---|---|
| $n$ | $\|B_D\varphi + u^i\|$ | $\tilde{\Lambda}_2$ | $\|B_D\varphi + u^i\|$ | $\tilde{\Lambda}_2$ |
| 1 | 88.88571 | 88.88571 | 88.88571 | 88.88571 |
| 2 | 15.43602 | 15.47797 | 15.43602 | 15.44441 |
| 3 | 7.98757 | 8.03549 | 7.97627 | 7.98588 |
| 4 | 4.27025 | 4.31695 | 4.25804 | 4.26742 |
| 5 | 2.30308 | 2.34531 | 2.29313 | 2.30163 |
| 10 | 0.10956 | 0.12661 | 0.10906 | 0.11249 |
| 11 | 0.06068 | 0.07446 | 0.06069 | 0.06347 |
| 12 | 0.03410 | 0.04519 | 0.03439 | 0.03663 |
| 13 | 0.01956 | 0.02847 | 0.02000 | 0.02179 |
| 14 | 0.01156 | 0.01869 | 0.01204 | 0.01347 |
| 15 | 0.00709 | 0.01280 | 0.00756 | 0.00870 |
| 20 | 0.00130 | 0.00316 | 0.00156 | 0.00194 |
| 25 | 0.00064 | 0.00124 | 0.00073 | 0.00085 |
| 29 | 0.00068 | 0.00093 | 0.00065 | 0.00070 |
| 30 | | | 0.00094 | 0.00098 |

Numerical results with $N_r = 5$ for each iterative method are presented in table 1 and figure 1 for the Newton-type method (NTM) and the gradient-type method (GTM). We considered an update factor for the GTM of $\delta = 10^{-3}$ for exact and $\delta = 5 \times 10^{-3}$ for noisy data.

*5.1.1. Influence of* $\eta_2$.

The influence of $\eta_2$ does not seem to affect much the accuracy of reconstructions of the gradient-type minimization with exact data, as we can see in table 2 and figure 2 for a rounded corner triangle. However, the

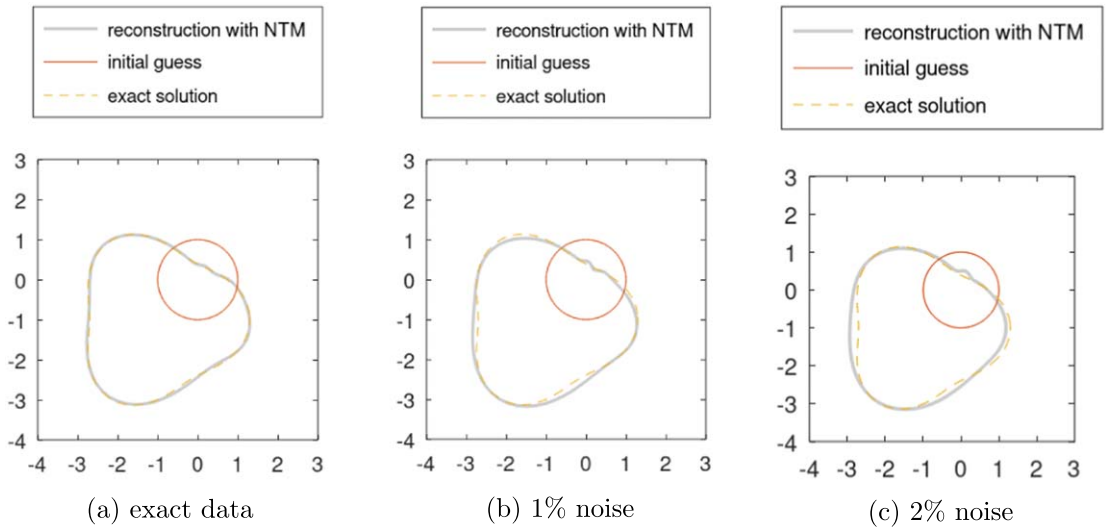


**Figure 3.** Reconstructions for the rounded corner triangle with displaced center in section 5.1.2 by the Newton-type approach for the second step of the Hybrid method.

**Table 3.** Sequence of values of $\tilde{\Lambda}_2(\gamma_n)$ with respect to the iteration $n$ by the Newton-type method (NTM) for the rounded triangle shaped scatterer with displaced center in section 5.1.2.

| $n$ | no noise | 1% noise | 2% noise |
|---|---|---|---|
| 1 | 100795.04138 | 507.84726 | 504.04643 |
| 2 | 23643.35049 | 227.18687 | 225.39684 |
| 3 | 7764.25337 | 73.57654 | 73.37209 |
| 4 | 1542.00411 | 7.70284 | 8.61337 |
| 5 | 377.09520 | 1.16315 | 2.39499 |
| 6 | 119.54710 | 1.01890 | 2.61771 |
| 7 | 31.70973 | 1.03298 | |
| 8 | 0.85288 | | |
| 9 | 0.17083 | | |
| 10 | 0.15890 | | |
| 11 | 0.14076 | | |
| 12 | 0.15223 | | |

use of a gradient-type method for a penalized cost function slightly affects the results with comparison to a non penalized Newton-approach for noisy data, as seen in the shown examples. Having this in mind we consider $\eta_2 = 0.8^{n-1} \times 10^{-2}$ for exact data and $\eta_2 = 0.8^{n-1}$ for noisy data.

*5.1.2. Obstacle with unknown center. TEXT*

Following remark 1, we now consider a domain with an unknown center, namely a rounded corner triangle centered at $(-1, 1)$ parametrized by

$$z(t) = (-1, -1) + (2 + 0.3\cos 3t)(\cos t, \sin t),\ t \in [2, \pi].$$

Numerical results for the Newton-type method are presented in table 3 and figure 3. In each iteration the first step is solved by Tikhonov regularization with a regularization parameter $\eta_1 = 0.8^{n-1} \times 10^{-8}$ for exact data and $\eta_1 = 0.8^{n-1} \times 10^{-2}$ for noisy data. For the first boundary approximation we considered a circumference centered at the origin, with radius 1.

### 5.2. Peanut

We now consider a peanut shaped domain (outside the approximation space) parameterized by

$$z(t) = 2\sqrt{\cos^2 t + 0.25\sin^2 t}\,(\cos t, \sin t),\ t \in [2, \pi].$$

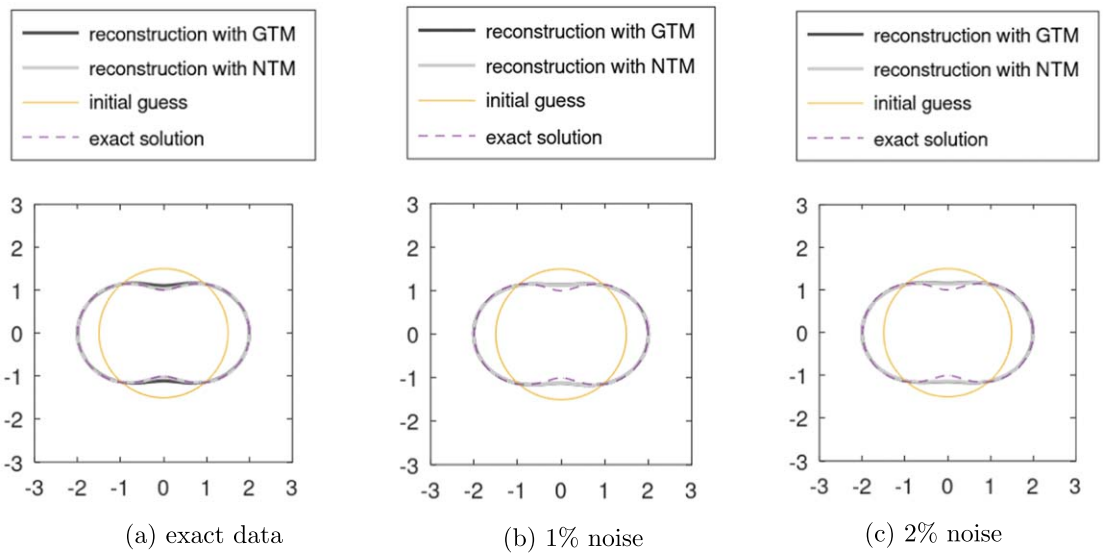


**Figure 4.** Reconstructions for the peanut shaped scatterer in section 5.2 by both approaches for the second step of the Hybrid method.

**Table 4.** Sequence of values of $\tilde{\Lambda}_2(\gamma_n)$ with respect to the iteration $n$ by the Newton-type method (NTM) and the gradient-type method (GTM) for the peanut shaped scatterer in section 5.2.

| | no noise | | 1% noise | | 2% noise | |
|---|---|---|---|---|---|---|
| $n$ | NTM | GTM | NTM | GTM | NTM | GTM |
| 1 | 18.93199 | 18.93199 | 14.76495 | 14.76495 | 14.78338 | 14.78338 |
| 2 | 0.26731 | 11.23584 | 0.83283 | 3.09606 | 0.83563 | 3.14217 |
| 3 | 0.00971 | 7.94393 | 0.31658 | 1.22527 | 0.33294 | 1.26491 |
| 4 | 0.00597 | 6.04503 | 0.28118 | 0.68321 | 0.30363 | 0.72579 |
| 5 | 0.00580 | 4.79789 | 0.26402 | 0.47827 | 0.29817 | 0.52593 |
| 6 | 0.00566 | 3.91113 | 0.25113 | 0.38267 | 0.29907 | 0.44033 |
| 8 | 0.00535 | 2.72684 | 0.23195 | 0.29746 | | 0.39242 |
| 9 | 0.00518 | 2.31150 | 0.22531 | 0.27517 | | 0.40024 |
| 12 | 0.00467 | 1.45834 | 0.22179 | 0.24660 | | |
| 13 | 0.00452 | 1.26145 | | 0.24855 | | |
| 21 | 0.00374 | 0.44003 | | | | |
| 22 | 0.00365 | 0.39008 | | | | |
| 23 | 0.00395 | 0.34663 | | | | |
| 24 | | 0.30860 | | | | |
| 30 | | 0.16034 | | | | |
| 37 | | 0.09118 | | | | |
| 38 | | 0.09171 | | | | |

Numerical results with $N_r = 5$ for each iterative method can be found in table 4 and figure 4 for the gradient-type method (GTM) and for the Newton-type method (NTM). We considered an update factor for the GTM of $\delta = 10^{-3}$ for exact and $\delta = 5 \times 10^{-3}$ for noisy data.

### 5.3. Kite

We now consider a more changelling geometry, namely the kite shape parameterized by

$$z(t) = (\cos t + 0.65 \cos 2t - 0.65,\ 1.5 \sin t),\ t \in [2,\ \pi]$$

Numerical results with $N_r = 20$ for each iterative method can be found in table 5 and figure 5for the gradient-type method (GTM) and for the Newton-type method (NTM). We considered an update factor for the GTM of $\delta = 10^{-3}$ for exact and $\delta = 5 \times 10^{-3}$ for noisy data.

### 5.4. Kite with $\kappa_D = 10 + 10i$

Finally we maintain the kite, but increase the interior wave number to $\kappa_D = 10 + 10i$. Numerical results for each iterative method can be found in table 6 and figure 6 for the gradient-type method (GTM) and for the Newton-

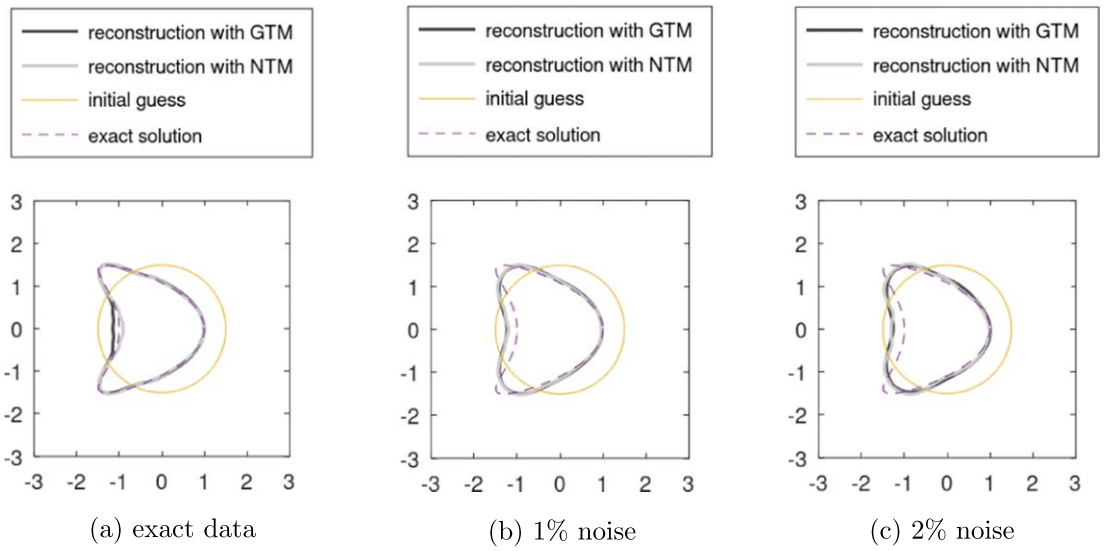


**Figure 5.** Reconstructions for the kite shaped scatterer in section 5.3 by both approaches for the second step of the Hybrid method.

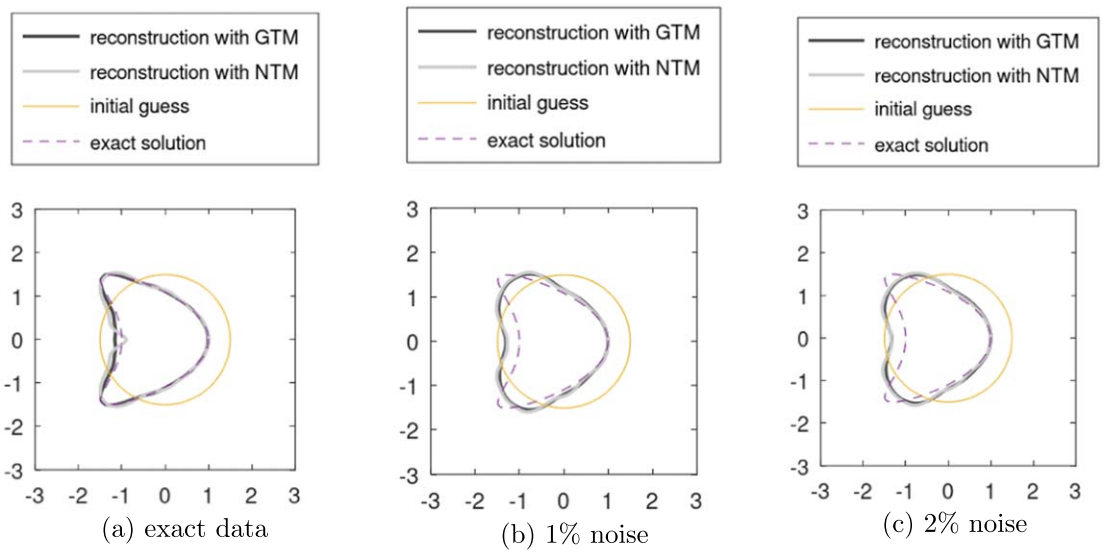


**Figure 6.** Reconstructions for the kite shaped scatterer with $\kappa_D = 10 + 10i$ in section 5.4 by both approaches for the second step of the Hybrid method.

**Table 5.** Sequence of values of $\tilde{\Lambda}_2(\gamma_n)$ with respect to the iteration $n$ by the Newton-type method (NTM) and the gradient-type method (GTM) for the kite shaped scatterer in section 5.3.

| | no noise | | 1% noise | | 2% noise | |
|---|---|---|---|---|---|---|
| $n$ | NTM | GTM | NTM | GTM | NTM | GTM |
| 1 | 28.61171 | 28.61171 | 18.26275 | 18.26275 | 18.56501 | 18.56501 |
| 2 | 6.14036 | 17.53459 | 3.73916 | 5.32985 | 4.05677 | 5.96212 |
| 3 | 0.69547 | 14.14543 | 1.18561 | 2.40052 | 1.80321 | 3.05500 |
| 4 | 0.23123 | 11.41312 | 1.16016 | 1.66871 | 1.86970 | 2.40778 |
| 5 | 0.17288 | 9.22041 | 1.20261 | 1.47066 | | 2.30618 |
| 6 | 0.15497 | 7.56645 | | 1.43195 | | 2.38020 |
| 7 | 0.14883 | 6.20041 | | 1.46149 | | |
| 8 | 0.14996 | 5.12504 | | | | |
| 9 | | 4.24806 | | | | |
| 10 | | 3.53494 | | | | |
| 20 | | 0.70429 | | | | |
| 30 | | 0.24349 | | | | |
| 35 | | 0.20610 | | | | |

**Table 6.** Sequence of values of $\tilde{\Lambda}_2(\gamma_n)$ with respect to the iteration $n$ by the Newton-type method (NTM) and the gradient-type method (GTM) for the kite shaped scatterer in section 5.4.

| | no noise | | 1% noise | | 2% noise | |
|---|---|---|---|---|---|---|
| $n$ | NTM | GTM | NTM | GTM | NTM | GTM |
| 1 | 30.09142 | 30.09142 | 17.14029 | 17.14029 | 17.29702 | 17.29702 |
| 2 | 7.76490 | 16.03483 | 4.21090 | 9.67171 | 4.23511 | 9.74979 |
| 3 | 1.86152 | 12.72052 | 3.16301 | 6.40780 | 3.09767 | 6.42674 |
| 4 | 1.15053 | 10.17757 | 3.05030 | 4.79135 | 2.98908 | 4.78308 |
| 5 | 1.16862 | 8.22575 | 2.98537 | 3.92285 | 2.95562 | 3.91160 |
| 6 | | 6.67985 | 2.93572 | 3.41665 | 2.92961 | 3.42234 |
| 7 | | 5.47770 | 2.83310 | 3.09640 | 2.88002 | 3.13757 |
| 8 | | 4.52179 | 2.74819 | 2.88032 | 2.85371 | 2.97501 |
| 9 | | 3.76217 | 2.67801 | 2.73200 | 2.86543 | 2.89842 |
| 10 | | 3.15437 | 2.62286 | 2.63589 | | 2.89215 |
| 11 | | 2.66538 | 2.60477 | 2.58515 | | 2.94889 |
| 12 | | 2.27004 | 2.61588 | 2.57504 | | |
| 13 | | 1.94888 | | 2.59985 | | |
| 20 | | 0.83198 | | | | |
| 30 | | 0.38029 | | | | |
| 37 | | 0.30049 | | | | |
| 38 | | 0.30554 | | | | |

type method (NTM). We considered an update factor for the GTM of $\delta = 10^{-3}$ for exact and $\delta = 2.5 \times 10^{-3}$ for noisy data.

## 6. Conclusion and further work

In this paper we generalized a hybrid method for inverse transmission problems and showed convergence for a related optimization problem. There is, however, a gap between the theoretical results and the practical application of the method, since the hybrid method divides the optimization in two steps, with fixed parameters in each, which may lead to a different minimum than if the optimization was performed for all the parameters at once. Nonetheless, numerical results seem to be feasible.

Also, we considered a Newton-type approach for the linearization of the second step and also a gradient-type method considering a penalization term on the oscillations of the solution. Numerical results show this term as few effect on the reconstruction, though reconstructions are feasible for both cases. This effect is more clear in figure 4 and figure 5 since the kite has a higher oscillating boundary. The paper was successful in extending the hybrid method from impenetrable to penetrable obstacles which can be seen as an iterative decomposition method for the transmission problem. However, the price to pay is that the transmission problem needs at least 8 incident directions for the hybrid method to perform well, while for the impenetrable case a unique incident direction was enough for accurate results [30, 31, 36, 37].

Future work might include extending the method to recover also a possibly unknown interior wavenumber $\kappa_D$, along with the shape of the scatterer, adapting the cost function with an extra input to this end. Extending the approach to 3D or other equations may also be challenging.

## Acknowledgments

Both authors are partially funded by FCT through the projects UIDB/04621/2020 (DOI: 10.54499/UIDB/04621/2020) and UIDP/04621/2020 (DOI: 10.54499/UIDP/04621/2020). Pedro Serranho is also partially funded by FCT through the projects UIDB/04950/2020 (DOI: 10.54499/UIDB/04950/2020) and UIDP/04950/2020 (DOI: 10.54499/UIDP/04950/2020).

## Data availability statement

No new data were created or analysed in this study.

## ORCID iDs

João Paixão https://orcid.org/0009-0003-4618-9881
Pedro Serranho https://orcid.org/0000-0003-2176-3923

## References

[1] Altundag A 2013 A hybrid method for inverse scattering problem for a dielectric *Advances in Applied Mathematics and Approximation Theory* ed G A Anastassiou and O Duman (Springer New York) 183–200
[2] Altundag A 2015 A second degree newton method for an inverse scattering problem for a dielectric cylinder *Hittite Journal of Science Engineering* **2** 115–25
[3] Altundag A and Kress R 2012 An iterative method for a two-dimensional inverse scattering problem for a dielectric *J. Inverse Ill-Posed Problems* **20** 575–90
[4] Alves C J S and Antunes P R S 2013 The method of fundamental solutions applied to some inverse eigenproblems *SIAM J. Sci. Comput.* **35** A1689–708
[5] Araújo A and Serranho P 2019 On the use of quasi-equidistant source points over the sphere surface for the method of fundamental solutions *J. Comput. Appl. Math.* **359** 55–68
[6] Arridge S 1999 Optical tomography in medical imaging *Inverse Problems* **15** R41–R93
[7] Barnett A H and Betcke T 2008 Stability and convergence of the method of fundamental solutions for helmholtz problems on analytic domains *J. Comput. Phys.* **227** 7003–26
[8] Borden B 1999 *Radar Imaging of Airborne Targets. A Primer for Applied Mathematicians and Physicists* 1st edn (Taylor & Francis) 158
[9] Colton D, Coyle J and Monk P 2000 Recent developments in inverse acoustic scattering theory *SIAM Rev.* **42** 369–414
[10] Colton D and Kress R 1983 *Integral Equation Methods in Scattering Theory* (Wiley)
[11] Colton D and Kress R 2017 Looking back on inverse scattering theory *OWP* **24** 779–807
[12] Colton D and Kress R 2019 *Inverse Acoustic and Electromagnetic Scattering Theory* 3rd edn (Springer) (https://doi.org/10.1007/978-1-4614-4942-3)
[13] Fairweather G, Karageorghis A and Martin P A 2003 The method of fundamental solutions for scattering and radiation problems *Eng. Anal. Bound. Elem.* **27** 759–69 Special issue on Acoustics
[14] Fang Z and Shixu M 2021 The interior inverse electromagnetic scattering for an inhomogeneous cavity *Inverse Problems* **37** 025007
[15] Farina D, Jiang Y and Dössel O 2009 Acceleration of fem-based transfer matrix computation for forward and inverse problems of electrocardiography *Med .Biol. Eng.Comput.* **47** 1229–36
[16] Isakov V 1990 On uniqueness in the invese transmission scattering problem *Commun. PDE* **15** 1565–86
[17] Ivanyshyn O and Kress R 2006 Nonlinear integral equations in inverse obstacle scattering *Mathematical Methods in Scattering Theory and Biomedical Engineering* **1** 39–50
[18] Ivanyshyn O, Kress R and Serranho P 2010 Huygens' principle and iterative methods in inverse obstacle scattering *Adv. Comput. Math.* **3** 413–29
[19] Yang B Z J and Zhang R 2012 A sampling method for the inverse transmission problem for periodic media *Inverse Problems* **28** 035004
[20] Kirsch A 1993 Numerical algorithms in inverse scattering theory *Ordinary and Partial Differential Equations* **IV** 93–111
[21] Kirsch A and Kress R 1986 On an integral equation of the first kind in inverse acoustic scattering *Inverse Problems (Cannon and Hornung, eds.), ISNM* **77** 93102
[22] Kirsch A and Kress R 1987 A numerical method for an inverse scattering problem *Engl and Groetsch, eds.), Academic Press, Orlando* **4** 279–90
[23] Kirsch A and Kress R 1987 An optimization method in inverse acoustic scattering *Boundary Elements IX, Vol.3 Fluid Flow and Potential Applications (Brebbia et al., eds), Springer Verlag, Berlin Heidelberg New York* **3** 3–18
[24] Kirsch A and Kress R 1993 Uniqueness in inverse obstacle scattering *Inverse Problems* **9** 285–99
[25] Kress R 1995 On the numerical solution of a hypersingular integral equation in scattering theory *J. Comp. Appl. Math.* **61** 345–60
[26] Kress R 1997 Integral equation methods in inverse acoustic and electromagnetic scattering *Boundary Integral Formulations for Inverse Analysis* **72** 6792
[27] Kress R 1998 *Numerical Analysis* (Springer) (https://doi.org/10.1007/978-1-4612-0599-9)
[28] Kress R 1999 *Linear Integral Equations* (Springer) (https://doi.org/10.1007/978-1-4614-9593-2)
[29] Kress R and Roach G F 1978 Transmission problems for the Helmholtz equation *J. Math. Phys.* **19** 1433–7
[30] Kress R and Serranho P 2005 A hybrid method for two-dimensional crack reconstruction *Inverse Problems* **21** 773–84
[31] Kress R and Serranho P 2007 A hybrid method for sound-hard obstacle reconstruction *J. Comput. Appl. Math.* **204** 418–27
[32] Lee K-M 2019 Inverse transmission scattering problem via a dirichlet-to-neumann map *Eng. Anal. Bound. Elem.* **101** 214–20
[33] Potthast R 1996 A survey on sampling and probe methods for inverse problems *Inverse Problems* **4** 67–84
[34] Potthast R 2006 Fréchet differentiability of the solution to the acoustic neumann scattering problem with respect to the domain *J. Inverse Ill-posed Prob.* **22** 67–84
[35] Ramm A G, Pang P Y H and Yan G 2000 A uniqueness result for the inverse transmission problem, number 5 *International Journal of Applied Math* **2** 625–34
[36] Serranho P 2006 A hybrid method for inverse scattering for shape and impedance *Inverse Problems* **22** 663–80
[37] Serranho P 2007 A hybrid method for inverse scattering for sound-soft obstacles in 3D *Inverse Problems Imaging* 691–712
[38] Smyrlis Y-S 2009 Applicability and applications of the method of fundamental solutions *Math. Comput.* **78** 1399–434
[39] Tant K, Galetti E, Mulholland A J, Curtis A and Gachagan A 2020 Effective grain orientation mapping of complex and locally anisotropic media for improved imaging in ultrasonic non-destructive testing *Inverse Prob. Sci. Eng.* **28** 1694–718
[40] Tikhonov A 1963 On the solution of incorrectly formulated problems and the regularization method *Soviet Math. Dokl.* **4** 1035–8
[41] Xiang J and Yan G 2021 Uniqueness of the inverse transmission scattering with a conductive boundary *Acta Mathematica Scientia* **41B** 925940